Wetting characteristics on hierarchical structures patterned by a femtosecond laser

2010 J. Micromech. Microeng. 20 075029

(http://iopscience.iop.org/0960-1317/20/7/075029)

J. Micromech. Microeng. 20 (2010) 075029 (8pp) doi:10.1088/0960-1317/20/7/075029

Wetting characteristics on hierarchical structures patterned by a femtosecond laser

Dongshi Zhang[1], Feng Chen[1], Guoping Fang[2], Qing Yang[1], Degang Xie[2], Guanjun Qiao[2], Wen Li[3], Jinhai Si[1] and Xun Hou[1]

[1] Key Laboratory of Photonics Technology for Information, Xi'an Jiaotong University, Xi'an 710049, People's Republic of China
[2] State Key Laboratory for Mechanical Behavior of Materials, Xi'an Jiaotong University, Xi'an 710049, People's Republic of China
[3] School of Materials Science and Engineering, Nanchang Hangkong University, Nanchang 330063, People's Republic of China

E-mail: chenfeng@mail.xjtu.edu.cn

Received 20 January 2010, in final form 30 April 2010
Published 14 June 2010
Online at stacks.iop.org/JMM/20/075029

Abstract
Micro-scale hierarchical structures consisting of parallel grooves decorated by embossed triangle patterns are prepared by femtosecond laser irradiation on silicon (Si) wafers. The effects of surface morphology on wetting properties are investigated, and the results show that increasing the vertex angle of the triangle and groove spacing will lead to the enhancement of wettability and anisotropy, respectively. The structured surfaces also exhibit high adhesive force with droplets remaining attached to the surface even when the sample is turned upside down. Furthermore, the evaporation process of a water droplet on such an anisotropic surface is characterized to study its dynamic wetting behavior.

(Some figures in this article are in colour only in the electronic version)

1. Introduction

The wettability of surfaces has received significant attention for its wide range of applications such as biochips, intelligent micro fluidics, lab-on-chip devices, sensor arrays and coatings for automotive and aerospace vehicles and self-cleaning surfaces [1–5]. Wetting characteristics of a surface can be greatly enhanced either by creating a rough surface on a hydrophobic material (physical method) or by modifying a rough surface with hydrophobic coatings (chemical method). Some chemical approaches have been widely employed such as silanization [6], fluorination [7], plasma treatment [8] and photolytic treatment [9]; however, some of these have the drawback of a short-lived effect, meaning that the hydrophobicity of the treated surfaces will deteriorate over time. Very often, surface roughening or patterning work together with chemical treatments to modify surface wettability by producing ordered or disordered surface structures, including photolithography [10], nanocasting and extruding of polymers [11], block copolymers [12], vertically aligned carbon nanotubes [13] and electron-beam lithography [14].

In comparison to these means, microstructuring by a femtosecond (fs) laser is specifically attractive from the perspectives of negligible heat-affected zone, precise ablation threshold and high resolution. A fs laser can be used for processing a wide range of materials such as metals, glasses, ceramics, etc especially for hardness, high melting point, resistance to corrosion and brittleness [15–17]. In addition, fabrication of true three-dimensional (3D) structures inside transparent materials is only possible by a nonlinear multiphoton absorption process of a high-intensity fs laser beam, thus allowing for their application in microfluidics and lab-on-chip devices [18–22]. Meanwhile, in combination with a precise three-dimensional computer number control (CNC) translation stage, fs laser micromachining provides a quick and efficient prototyping means which enables us to fulfill the fabrication of structures with small and fine features in the micro–nano scale being independent of expensive masks and clean room.

There have been a few studies concerning the preparation of hydrophobic surfaces using fs laser pulses. Baldacchini *et al* [23] initially created superhydrophobic laser-structured silicon surfaces by coating a layer of fluoroalkylsilane molecules, while Zorba *et al* [24, 25] reported the wettability and water motion behavior of Si surfaces consisting of periods of conical spikes induced by fs laser irradiation in gaseous SF_6; meanwhile, they also investigated the self-cleaning and water repellent properties of these surfaces [26]. Kietzig *et al* [27] analyzed the wetting behavior of different metal alloys irradiated with a fs laser at different fluence and pointed out that the alloys with initially smooth, hydrophilic surfaces could become nearly superhydrophobic or even superhydrophobic over time. Wu *et al* [28] used low laser fluence to fabricate typical laser-induced periodic surface structures (LIPSS) on stainless steel surfaces with a submicron level to achieve superhydrophobic surfaces with a maximal contact angle (CA) of 166.3°. Yoon *et al* [29] utilized a fs laser to create a poly(dimethylsiloxane) (PDMS) mold with dual scale roughness, which exhibits superhydrophobicity, for the negative and positive replica of the structure on PDMS to check the reproductive wettability. But till now, to the best of our knowledge, no report has been reported on other wetting characteristics of a hydrophobic surface patterned by a fs laser, such as anisotropy, high adhesive force and droplet evaporation process.

In this paper, we report for the first time on the multiple wetting characteristics of hydrophobic silicon surfaces patterned by fs laser micromachining. By means of tuning the groove spacing, the structures allow one to tune the anisotropic wettability on Si wafers. The structured hydrophobic surfaces also exhibited high adhesive force with a drop remaining attached to the surface even under the condition of turning the sample upside down. Furthermore, the evaporation process of a 2 μl water droplet on an anisotropic hydrophobic surface was characterized to analyze dynamic wetting behavior.

2. Experiments

2.1. Experimental setup

The laser source was a Ti:sapphire oscillator–amplifier system (FEMTOPOWER Compact Pro, Austria), which delivered 800 nm, 30 fs Gaussian laser pulses at a repetition rate of 1 kHz. The sample was positioned on a high-precision *X–Y–Z* translation stage (computer controlled) perpendicular to the incident laser beam. A mechanical shutter was synchronized to the translation stages for turning the laser beam on and off. The laser beam was attenuated and then focused onto the sample using a 20× microscope objective (Nikon, NA = 0.45). Each sample was fabricated with a constant average power of 7 mW at a scanning speed of 1 mm s^{-1}, in which case the laser spot size is 9 μm. The morphology of the corresponding textured silicon surfaces was characterized by scanning electron microscopy (SEM), an optical microscope (LV100D, Nikon) and a confocal microscope (VK-9700, KEYENCE). Prior to the CA measurement, samples were ultrasonically cleaned in acetone, ethanol and deionized water in this sequence. The static CA was measured at room temperature by the sessile drop method with a Dataphysics OCA20 CA analyzer using a 2 μl deionized water drop. The digital drop image was processed by an image analysis system which calculated both the left and right contact angles from the shape of the drop with an accuracy of ±0.1°. The mean CA value was calculated from at least three individual measurements.

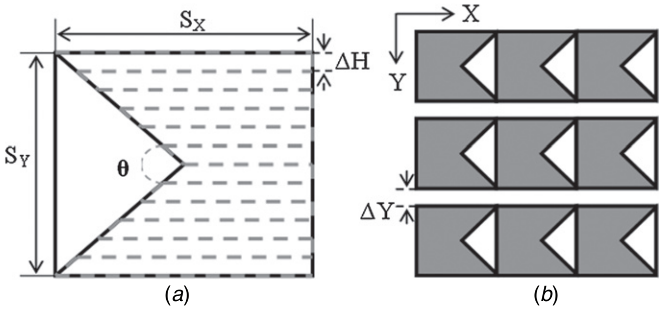

Figure 1. Schematic illustration of the fabrication of hierarchical structure. (*a*) Parallel linear scanning method to obtain an embossed triangle. (*b*) Periodic embossed triangle array separated by grooves.

2.2. Fabrication of hierarchical structures

Figure 1 shows the schematic representation of the processing steps for fabricating periodic arrays of embossed triangle structures separated by parallel grooves. The parallel linear scanning method is employed to form a triangle pattern, as denoted by dashed lines in figure 1(*a*). In order to ensure full ablation [30, 31], the interval between adjacent laser scanning lines ΔH was kept constant at 2 μm in our experiments. Then through layer-by-layer ablation, the pattern with different depths and a smooth shape [32] could be achieved. The layer space was set at 20 μm and the number of ablation layers was set at three. The triangle surface structure is characterized by the vertex angle θ, the width S_X, the height S_Y and the groove spacing ΔY (figures 1(*a*) and (*b*)). The parameter θ and the groove spacing ΔY were independently varied to investigate the effects of morphology on wettability, with S_X and S_Y kept constant at 200 μm.

3. Results

3.1. Morphology

Figures 2(*a*) and (*b*) show the SEM images of the microstructured silicon surface consisting of periods of embossed triangle patterns arranged in square lattices with different vertex angles. The local amplification images are shown in figures 2(*c*) and (*d*). The morphology of the ablated surface in Si consists of self-organized conical spike forests with characteristic sizes from tens of μm, decorated by fine features between tens and a few hundreds of nm, which resembles that of a natural lotus leaf, resulting in a significant increase in the overall roughness. The spike

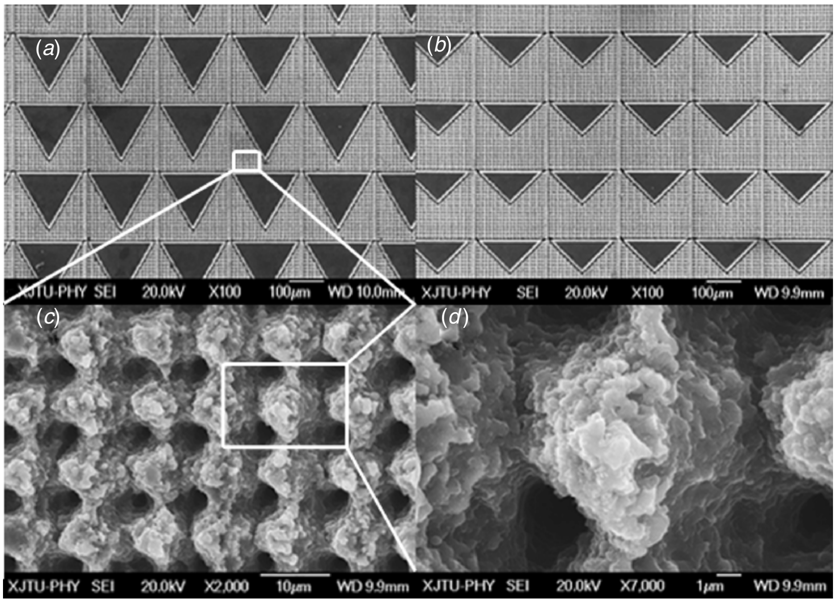

Figure 2. SEM images of grooved structures fabricated by a femtosecond laser on Si with the groove spacing ΔY of 8 μm. The vertex angle of the triangle patterns is different with S_X and S_Y both 200 μm: (*a*) $\theta = 60^\circ$ and (*b*) $\theta = 120^\circ$. SEM images of structures in the corresponding position: (*c*) low magnification and (*d*) high magnification.

density and average spike spacing are consistent due to the fixed value of scanning velocity and laser power. The spikes are roughly separated by 10 μm (figure 2(*d*)) with height stabilizing around 10 μm obtained by the image processing algorithm. Cones with morphology similar to the ones we observed have been seen by other authors on silicon under SF_6 or Cl_2 gas conditions [33] or under water ablation [34]. Their formation results from the following mechanism: first, submicrometer-sized ripple structures form on the smooth silicon surface, and then when adjacent scanning line passes by, the overlapped process region becomes coarser leading to formation of micrometer-scale ridges on top of the ripples. Subsequently, through layer-by-layer treatment, the coarsened layer breaks up into micrometer-sized beads, and subsequently evolves into spikes.

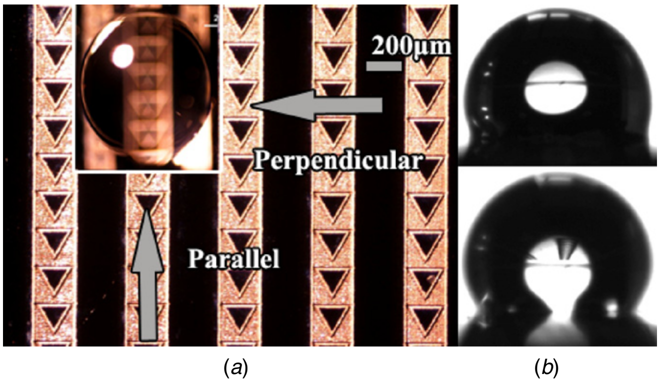

Figure 3. Schematic for the directional measurement of contact angles on structures. (*a*) Topographical image of the grooved structure. (*b*) Side views of a sessile drop on the surface from the parallel (bottom) and perpendicular (top) directions, respectively.

3.2. Anisotropic wetting characterization

If a surface shows identical contact angles when measured from different directions, the surface is defined as isotropic in wettability; otherwise it is anisotropic. The schematic for the measurement of anisotropic wetting of a water drop on the grooved surface is shown in figure 3. The top view indicates the elongation of the water drop along the grooved structure, and the side views show the cross-sectional shapes from two orthogonal directions parallel and perpendicular to the direction defined by the grooves. The difference between the CA values measured from the parallel (par) direction and those measured from the perpendicular (per) direction is defined as the degree of wetting anisotropy ($\Delta\theta$).

As shown in figure 4(*a*), the CA measured from par-direction ($\theta_\parallel$) increases from 140° to 145°, accompanied by the CA measured from the per-direction ($\theta_\perp$) increasing from 137°to 145°, with the increase of the vertex angle of the triangle pattern. Figure 4(*b*) shows the relationship between CA and the groove spacing. It is observed that when the groove spacing increases from 8 μm to 300 μm, $\theta_\perp$ decreases dramatically from 138° to 110°, while $\theta_\parallel$ declines slowly from 140° to 127°, resulting in an increase in the wetting anisotropy $\Delta\theta$ from 2° to 17°.

In order to understand the response of the structures, one has to consider the effect of the macroscopic surface roughness on the wettability, which has been theoretically explained by two different models. In the Wenzel model [35], the liquid drop is assumed to totally penetrate within the structured surface, described as the 'homogeneous wetting regime', and the liquid–solid CA θ_w follows the equation

$$\cos\theta_W = r\cos\theta_Y, \tag{1}$$

where r is the surface ratio between the overall surface area and the projected structured surface, and it equals 1 for a smooth

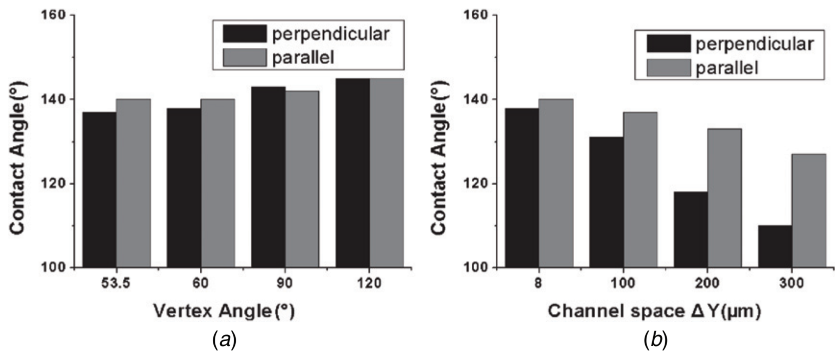

Figure 4. Static anisotropic wetting characteristics of grooved surfaces under different conditions: (*a*) vertex angle from 53.5° to 120° with the groove spacing ΔY of 8 μm and (*b*) the groove spacing from 8 μm to 300 μm.

surface and has a value greater than 1 for a rough surface, and θ_Y denotes the liquid CA on a flat surface.

In contrast, the Cassie and Baxter (C–B) model assumes that the liquid drop does not completely wet the structured surface but interacts with the composite surface made of a substrate material and air which is trapped in the crevices of the structured surface [36]. In this configuration, the CA θ_{CB} is given by

$$\cos\theta_{\mathrm{CB}} = f\cos\theta_Y + f - 1. \tag{2}$$

In the above expression, f is the fraction of the solid–liquid interface and $(1-f)$ is that of the solid–air interface. Whether a water drop exists in the Wenzel state or in the C–B state can be speculated by CA hysteresis [37–39]. The CA hysteresis has an extremely small value in the C–B state, while it takes a very large value in the Wenzel state. From the hysteresis values mentioned below, it seems that the Wenzel state should be favored in our results; but considering that the CA value of the unstructured Si surface is 61°, it is indicated that the Si surface is intrinsic hydrophilic. As for the Wenzel model, the hydrophilic surface becomes more hydrophilic after the structuring of the surface for the increment of the roughness factor r in equation (1), revealing a rigorous deviation from our experimental results which exhibit hydrophobicity. With respect to the fully textured surface consisting of spikes without any groove and triangle pattern, the CA value is 154°. Consequently, the surface is supposed to abide by the combined Cassie–Wenzel model [40–43].

Assuming that the surface with hierarchical structures is composed of two materials, one is fs structured spikes with $\theta_1 = 154°$, the other is hydrophilic Si with $\theta_2 = 61°$. The CA on the composite surface could be solved by the C–B equation [36]

$$\cos(\theta) = f_1\cos(\theta_1) + f_2\cos(\theta_2). \tag{3}$$

It is generally considered that f_1 and f_2 are defined as the liquid–solid interfacial contact area fractions for each material. But recently, many researchers have suggested that only the composition of the surface at the triple-contact line, not the contact area, controls the wetting of heterogeneous surfaces [44–46], and it has been proven by experiments [47].

To identify the true wetting behavior of the composite surfaces, the triple line model is put forward. It is generally regarded that an ellipse is the ideal contact line geometry of a drop sitting on an anisotropic surface, but owing to the pinning of the triangular base line, the squeezing of the apex of the triangle leading to the droplet's tendency to land on the triangle's base line and the influence of the side edges of triangles (figure 6(*b*)), the droplet gets distorted. Through observation of droplet evaporation on such structures (section 3.3), the approximate triple line is depicted in figure 5, as illustrated by a red line. In order to facilitate calculation, the triple line of the untextured groove's contact line is assumed to be straight lines and the contact line pins triangle edges derives from the effect of spikes. Therefore, the line ratio of the unstructured Si surface f_2 and spikes f_1 can be calculated using

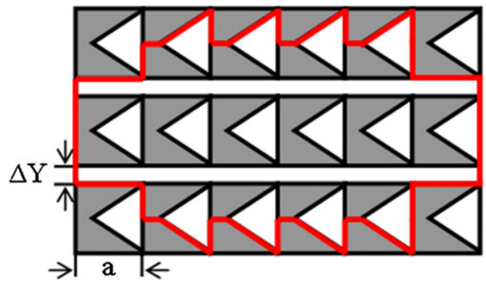

Figure 5. The triple line model on embossed triangle patterns.

Table 1. The line ratios for the unstructured Si surface (f_1), spikes (f_2) and corresponding contact angle.

Sample	Triple line model		
ΔY (μm)	f_1	f_2	θ (°)
100	0.91	0.09	140
200	0.84	0.16	133
300	0.78	0.22	126

$$f_2 = \frac{2\Delta Y}{2\Delta Y + 10.532a}, \tag{4}$$

$$f_1 = 1 - f_2, \tag{5}$$

where ΔY is the groove spacing and a is the square lattice length constant of 200 μm. The resulting contact line fractions f_1 and f_2 and the corresponding CAs calculated from equation (3) are listed in table 1.

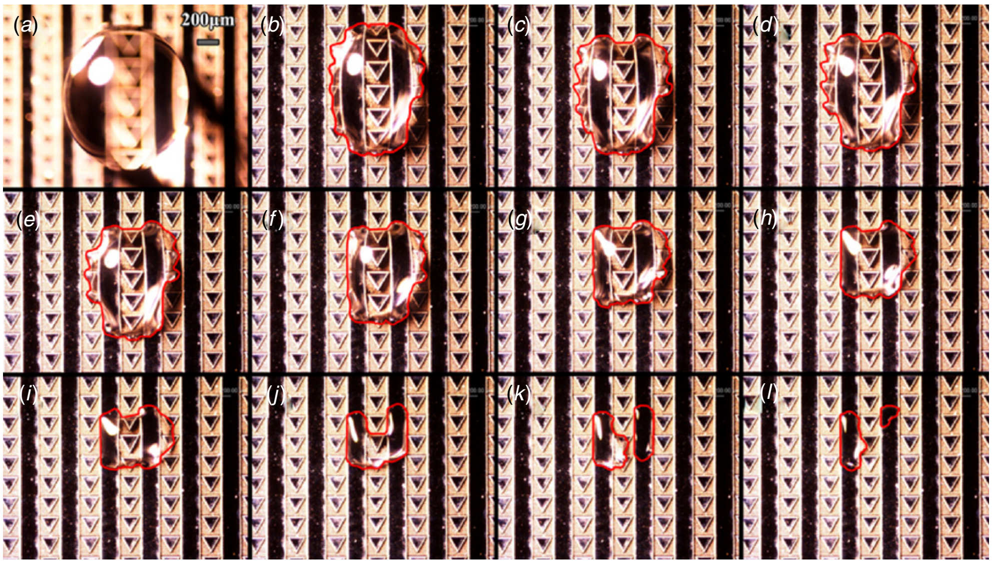

Figure 6. 5× microscopic image sequences illustrating evaporation of a 2 μl water droplet on the modified surface with the groove spacing of 200 μm with (*a*)–(*l*) corresponding to the times 0 s, 720 s, 780 s, 840 s, 900 s, 960 s, 1020 s, 1080 s, 1140 s, 1170 s, 1190 s and 1200 s, respectively.

The results demonstrate that a hydrophilic flat Si surface could become hydrophobic after laser micromachining periodic spikes and the wettability of the composite surface will decrease with increasing groove width, in agreement with our results of $\theta_{\|}$ (figure 4(*b*)) in general. The little difference may be on account of the approximation of the untextured groove contact line (it should be a curve, not a straight line in calculations) and contact line bending of the unstructured Si surface on the embossed triangles. The anisotropic wettability stems from macro patterns such as parallel grooves and triangles, and especially from parallel grooves, which have been investigated by many researchers [48–50], due to their 'squeezing' effect as featured by contact line pinning on the edge of the surface and generation of more energy barriers between multiple metastable states along the grooves, which cause less preference for a liquid to spread from per-direction, resulting in a higher static CA along the parallel direction. The periodic spikes in a micro-scale act as clamps which pin the droplet among them, resulting in the transition of the surface from hydrophilic to hydrophobic. The enhancement of the wettability in figure 4(*a*) can be attributed to the rise in pinning effect by increasing the number of spikes with an increase in the vertex angle of the triangle pattern. The nano-scale protrusions decorated on the spikes, especially on the ones in the lower location, may prop a droplet up, making the liquid drop unable to wet the bottom of the holes among the spikes, thus leading to incomplete penetration of the spikes.

3.3. Evaporation of a water droplet on the anisotropic hydrophobic surface

There have been some reports analyzing the characterization of the evaporation of droplets on isotropic superhydrophobic surfaces [51, 52], but only one observation of droplet evaporation phenomena on anisotropic wetting surfaces with parallel grooves [53]. For comparison, the evaporation process of a droplet on a surface with parallel grooves decorated by embossed triangle structures is captured and presented. By analyzing the shape variations of the droplet during evaporation, the effect of the triangle pattern on the pinning of the contact line is studied. The sample is placed on a flat sample stage equipped on an optical microscope. Light is provided by a light source (SCHOTT KL1500 LCD) with two external flexible fiber optic arms. Images are begun to be taken by a CCD camera before the droplet is placed and ended after evaporation is concluded.

Figure 6 shows image sequences of evaporation of a 2 μl water droplet on the modified surface with (*a*)–(*l*) corresponding to the times 0 s, 720 s, 780 s, 840 s, 900 s, 960 s, 1020 s, 1080 s, 1140 s, 1170 s, 1190 s and 1200 s, respectively. The water droplet initially has a regular oval shape (figure 6(*a*)), acting as a lens so that we cannot focus on the triple-phase (liquid–air-solid) contact line (TCL). As the evaporation proceeds, the CA $\theta_{\perp}$ changes dramatically as the height of the droplet decreases, while the contact line remains intact, thus enabling us to view the TCL perpendicular to the grooves, that is the bottom of the triangle pattern (figure 6(*b*)). Subsequently, by capturing the evaporation image with $\theta_{\|}$ close to 90°, we can clearly see the TCL parallel to the grooves, as shown in figure 6(*c*), where the TCL on the down-right hand recedes a little, while the left TCL remains well. Consequently, these clearly demonstrate that there exists a more continuous and shorter TCL along the parallel direction than that along the perpendicular direction, which offers us an insight into understanding why this structure exhibits anisotropy.

The pattern of light visible beneath the droplet indicates that the droplet sits on five square lattices of 1000 μm along the parallel direction and possesses two grooves and almost two square lattices amounting to 800 μm along the perpendicular direction (figure 6(*c*)). As the evaporation progresses with $\theta_{\|}$ less than 90°, the droplet size decreases in both directions.

Figure 7. Shapes of the water droplets on the microstructures with $\Delta Y = 100\ \mu$m, as seen from the per-direction at tilt angles of (*a*) 0°, (*b*) 90° and (*c*) 180°.

The droplet initially retreats from the bottom margin or side edge of the triangle structure on the down-left and up-left hand to the center, and anchors on the area close to the side of an adjacent triangle or attaches to the adjacent groove, as shown in figures 6(*d*) and (*e*), due to the surface energy difference or the changing slope of the film [54], known as pinning, having been shown on wettability defects leading to substantial deformations of the contact line [55, 56]. Subsequently, the parts of the droplet sitting on the left triangle patterns all retract to the groove edge for the tension being produced by simultaneous shrinkage from down-left and up-left sides and the metastable states resulting from the discontinuity of the contact line made up of the spikes and triangles' side edges, and accompany the water recession of half of square length along the parallel direction (figure 6(*f*)). The time period of 960 s to 1140 s also follows the procedures mentioned above with shrinkage along the directions from the down-right part of the droplet to the center and from the triangle apex to its bottom. As the evaporation progresses, the droplet volume becomes smaller and the evaporation speed accelerates, especially during the last minute (figures 6(*j*)–(*l*)) when the droplet initially recedes from the triangle bottom to its crest and then collapses into two parts and finally disappears. More interestingly, a new shape just like an 'apple' appears as the evaporation proceeds due to the depinning of the contact line. The whole evaporation process suggests that the fluid shrinks selectively from the triangle apex to its bottom (780–1140 s) or in the opposite direction (1140–1170 s), distinctive from simultaneous shrinkage of rectangular shaped parallel grooves from both ends. Drying phenomena like this may be of use in the fields of self-assembly to form aligned arrays of nanomaterials such as DNA [57] and CNT [58].

3.4. *High adhesive force*

Recently, more attention has been given to the preparation of a hydrophobic surface with high CA hysteresis for maintaining the position of a nearly spherical drop of water on the substrate [59, 60]. Such hydrophobic surfaces with sufficiently high adhesive force have unique advantages of meeting the increasing needs of controlled transport of small amount of liquids in biochemical separation, targeted drug delivery and immunoassay for open microfluidic devices.

Figures 7(*a*)–(*c*) show the behavior of the water droplet when the sample is laid flat, tilted vertically and turned upside down with the drop remaining attached to the surface. The mechanism of this phenomenon could be ascribed to the combined Cassie–Wenzel model in which the droplet is able to wet the surface and pins in the voids between the spike periods (figure 2(*c*)), thus resulting in a high CA hysteresis and making the surface become 'sticky'.

4. Conclusions

In conclusion, we have presented a new type of micro-scale hierarchical structure based on fs laser micromachining of Si wafers. The dependence of wetting properties on surface morphology without deposition of hydrophobic coatings is examined. The results show that the vertex angle of the triangle has little influence on the wetting characteristics, while by varying the groove spacing, one can easily control the anisotropy of the structured surface. The hydrophobic surfaces also exhibit high adhesive force owing to the periodic spikes, even when the sample is turned upside down. As a consequence, laser structuring can be utilized to control wetting characteristics and immobilization. The simplicity of the structuring process, together with CNC, renders this technique a powerful tool for tailoring the wetting response of a surface in microfluidic devices, formation of anisotropic nanomaterials and self-cleaning surface applications.

Acknowledgments

The authors gratefully acknowledge the financial support for this work provided by the National High Technology R&D Program of China under the grant no 2009AA04Z305 and National Science Foundation of China under the grant nos 60678011 and 10674107.

References

[1] Blossey R 2003 Self-cleaning surfaces—virtual realities *Nat. Mater.* **2** 301–6

[2] Callies M and Quere D 2005 On water repellency *Soft Matter* **1** 55–61

[3] Velev O D, Prevo B G and Bhatt K H 2003 On-chip manipulation of free droplets *Nature* **426** 515–6

[4] Verplanck N, Coffinier Y, Thomy V and Boukherroub R 2007 Wettability switching techniques on superhydrophobic surfaces *Nanoscale Res. Lett.* **2** 577–96

[5] Zorba V, Stratakis E, Barberoglou M, Spanakis E, Tzanetakis P, Anastasiadis S H and Fotakis C 2008 Biomimetic artificial surfaces quantitatively reproduce the water repellency of a lotus leaf *Adv. Mater.* **20** 4049–54

[6] Almanza-Workman A M, Raghavan S, Deymier P, Monk D J and Roop R 2002 Water dispersible silanes for wettability modification of polysilicon *J. Electrochem. Soc.* **1491** H6–11

[7] Colorado R and Lee T R 2003 Wettabilities of self-assembled monolayers on gold generated from progressively fluorinated alkanethiols *Langmuir* **19** 3288–96

[8] Guruvenket S, Rao G M, Komath M and Raichur A M 2004 Plasma surface modification of polystyrene and polyethylene *Appl. Surf. Sci.* **236** 278–84

[9] Athanassiou A, Lygeraki M L, Pisignano D, Lakiotaki K, Varda M, Mele E, Fotakis C, Cingolani R and Anastasiadis S H 2006 Photocontrolled variations in the wetting capability of photochromic polymers enhanced by surface nanostructuring *Langmuir* **22** 2329–33

[10] Shirtcliffe N J, Aqil S, Evans C, McHale G, Newton M I, Perry C C and Roach P 2004 The use of high aspect ratio photoresist (SU-8) for super-hydrophobic pattern prototyping *J. Micromech. Microeng.* **14** 1384–9

[11] Feng L, Li S, Li H, Zhai J, Song Y, Jiang L and Zhu D 2002 Super-hydrophobic surface of aligned polyacrylonitrile nanofibers *Angew. Chem. Int. Ed.* **41** 1221–3

[12] Xie Q, Fan G, Zhao N, Guo X, Xu J, Dong J, Zhang L, Zhang Y and Han C C 2004 Facile creation of a bionic super-hydrophobic block copolymer surface *Adv. Mater.* **16** 1830–3

[13] Lau K K S, Bico J, Teo K B K, Chhowalla M, Amaratunga G A J, Milne W I, McKinley G H and Gleason K K 2003 Superhydrophobic carbon nanotube forests *Nano Lett.* **3** 1701–5

[14] Martines E, Seunarine K, Morgan H, Gadegaard N, Wilkinson C D W and Riehle M 2005 Super-hydrophobicity and super-hydrophilicity of regular nanopatterns *Nano Lett.* **5** 2097–103

[15] Sano T, Yanai M, Ohmura E, Nomura Y, Miyamoto I, Hirose A and Kobayashi K F 2005 Femtosecond laser fabrication of microspike-arrays on tungsten surface *Appl. Surf. Sci.* **247** 340–6

[16] Torchia G A, Meilan P F, Rodenas A, Jaque D, Mendez C and Roso L 2007 Femtosecond laser written surface waveguides fabricated in Nd:YAG ceramics *Opt. Express* **15** 13266–71

[17] Farson D F, Choi H W, Zimmerman B, Steach J K, Chalmers J J, Olesik S V and Lee L J 2008 Femtosecond laser micromachining of dielectric materials for biomedical applications *J. Micromech. Microeng.* **18** 035020

[18] Sugioka K, Cheng Y and Midorikawa K 2005 Three-dimensional micromachining of glass using femtosecond laser for lab-on-a-chip device manufacture *Appl. Phys.* A **81** 1–10

[19] Masuda M, Sugioka K, Cheng Y, Hongo T, Shihoyama K, Takai H, Miyamoto I and Midorikawa K 2004 Direct fabrication of freely movable microplate inside photosensitive glass by femtosecond laser for lab-on-chip application *Appl. Phys.* A **78** 1029–32

[20] Hanada Y, Sugioka K, Kawano H, Ishikawa I S, Miyawaki A and Midorikawa K 2008 Nano-aquarium for dynamic observation of living cells fabricated by femtosecond laser direct writing of photostructurable glass *Biomed. Microdevices* **10** 403–10

[21] Hanada Y, Sugioka K and Midorikawa K 2008 Selective metallization of photostructurable glass by femtosecond laser direct writing for biochip application *Appl. Phys.* A **90** 603–7

[22] Kim M, Hwang D J, Jeon H, Hiromatsu K and Grigoropoulos C P 2009 Single cell detection using a glass-based optofluidic device fabricated by femtosecond laser pulses *Lab Chip* **9** 311–8

[23] Baldacchini T, Carey J E, Zhou M and Mazur E 2006 Superhydrophobic surfaces prepared by microstructuring of silicon using a femtosecond laser *Langmuir* **22** 4917–9

[24] Zorba V, Persano L, Pisignano D, Athanassiou A, Stratakis E, Cingolani R, Tzanetakis P and Fotakis C 2006 Making silicon hydrophobic wettability control by two-lengthscale simultaneous patterning with femtosecond laser irradiation *Nanotechnology* **17** 3234–8

[25] Zorba V, Stratakis E, Barberoglou M, Spanakis E, Tzanetakis P and Fotakis C 2008 Tailoring the wetting response of silicon surfaces via fs laser structuring *Appl. Phys.* A **93** 819–25

[26] Barberoglou M, Zorba V, Stratakis E, Spanakis E, Tzanetakis P, Anastasiadis S H and Fotakis C 2009 Bio-inspired water repellent surfaces produced by ultrafast laser structuring of silicon *Appl. Surf. Sci.* **255** 5425–9

[27] Kietzig A M, Hatzikiriakos S G and Englezos P 2009 Patterned superhydrophobic metallic surfaces *Langmuir* **25** 4821–7

[28] Wu B, Zhou M, Li J, Ye X, Li G and Cai L 2009 Superhydrophobic surfaces fabricated by microstructuring of stainless steel using a femtosecond laser *Appl. Surf. Sci.* **256** 61–6

[29] Yoon T O, Shin H J, Jeoung S C and Park Y-I 2008 Formation of superhydrophobic poly(dimethysiloxane) by ultrafast laser-induced surface modification *Opt. Express* **16** 12715–25

[30] Liao Y, Xu J, Sun H, Song J, Wang X and Cheng Y 2008 Fabrication of microelectrodes deeply embedded in $LiNbO_3$ using a femtosecond laser *Appl. Surf. Sci.* **254** 7018–21

[31] Bellouard Y, Said A, Dugan M and Bado P 2004 Fabrication of high-aspect ratio, micro-fluidic channels and tunnels using femtosecond laser pulses and chemical etching *Opt. Express* **12** 2120–9

[32] Kamlage G, Bauer T, Ostendorf A and Chichkov B N 2003 Deep drilling of metals by femtosecond laser pulses *Appl. Phys.* A **77** 307–10

[33] Her T-H, Finlay R J, Wu C, Deliwala S and Mazur E 1998 Microstructuring of silicon with femtosecond laser pulses *Appl. Phys. Lett.* **73** 1673–5

[34] Shen M Y, Crouch C H, Carey J E and Mazur E 2004 Femtosecond laser-induced formation of submicrometer spikes on silicon in water *Appl. Phys. Lett.* **85** 5694–6

[35] Wenzel R N 1936 Resistance of solid surfaces to wetting by water *Ind. Eng. Chem.* **28** 988–94

[36] Cassie A B D and Baxter S 1944 Wettability of porous surfaces *Trans. Faraday Soc.* **40** 546–51

[37] Marmur A 2003 Wetting on hydrophobic rough surfaces: to be heterogeneous or not to be? *Langmuir* **19** 8343–8

[38] Quere D 2005 Non-sticking drops *Rep. Prog. Phys.* **68** 2495

[39] Marmur A 2006 Soft contact: measurement and interpretation of contact angles *Soft Matter* **2** 12–7

[40] Narhe R D and Beysens D A 2004 Nucleation and growth on a superhydrophobic grooved surface *Phys. Rev. Lett.* **93** 076103

[41] Wier K A and McCarthy T J 2006 Condensation on ultrahydrophobic surfaces and its effect on droplet mobility: ultrahydrophobic surfaces are not always water repellant *Langmuir* **22** 2433–6

[42] Dorrer C and Ruhe J 2007 Condensation and wetting transitions on microstructured ultrahydrophobic surfaces *Langmuir* **23** 3820–4

[43] Ran C, Ding G, Liu W, Deng Y and Hou W 2008 Wetting on nanoporous alumina surfaces: transition between Wenzel

and Cassie states controlled by surface structure *Langmuir* **24** 9952–5

[44] Extrand C W 2003 Contact angles and hysteresis on surfaces with chemically heterogeneous islands *Langmuir* **19** 3793–6

[45] Hey M J and Kingston J G 2007 The apparent contact angle for a nearly spherical drop on a heterogeneous surface *Chem. Phys. Lett.* **447** 44–8

[46] Cubaud T and Fermigier M 2004 Advancing contact lines on chemically patterned surfaces *Colloid Interface Sci.* **269** 171–7

[47] Larsen S T and Taboryski R 2009 A Cassie-like law using triple phase boundary line fractions for faceted droplets on chemically heterogeneous surfaces *Langmuir* **25** 1282–4

[48] Liu L, Jacobi A M and Chvedov D 2009 A surface embossing technique to create micro-grooves on an aluminum fin stock for drainage enhancement *J. Micromech. Microeng.* **19** 035026

[49] Johnson R E Jr and Dettre R H 1964 Contact angle hysteresis: I. Study of an idealized rough surface *Adv. Chem. Ser.* **43** 112–35

[50] Johnson R E Jr and Dettre R H 1964 Contact angle hysteresis: III. Study of an idealized heterogeneous surface *J. Phys. Chem.* **68** 1744–50

[51] McHale G, Aqil S, Shirtcliffe N J, Newton M I and Erbil H Y 2005 Analysis of droplet evaporation on a superhydrophobic surface *Langmuir* **21** 11053–60

[52] McLauchlin M L, Yang D, Aella P, Garcia A A, Picraux S T and Hayes M A 2007 Evaporative properties and pinning strength of laser-ablated, hydrophilic sites on lotus-leaf-like, nanostructured surfaces *Langmuir* **23** 4871–7

[53] Xia D and Brueck S R J 2008 Strongly anisotropic wetting on one-dimensional nanopatterned surfaces *Nano Lett.* **8** 2819–24

[54] Kalinin Y V, Berejnov V and Thorne R E 2009 Contact line pinning by microfabricated patterns: effects of microscale topography *Langmuir* **25** 5391–7

[55] Cubaud T, Fermigier M and Jenffer P 2001 Spreading of large drops on patterned surfaces *Oil Gas Sci. Technol.* **56** 23–31

[56] Marsh J A and Cazabat A M 1993 Dynamics of contact line depinning from a single defect *Phys. Rev. Lett.* **71** 2433–6

[57] Fang X, Li B, Petersen E, Seo Y S, Samuilov V A, Chen Y, Sokolov J C, Shew C Y and Rafailovich M H 2006 Drying of DNA droplets *Langmuir* **22** 6308–12

[58] Li Q, Zhu Y T, Kinloch I A and Windle A H 2006 Self-organization of carbon nanotubes in evaporating droplets *J. Phys. Chem.* B **110** 13926–30

[59] Winkleman A, Gotesman G, Yoffe A and Naaman R 2008 Immobilizing a drop of water: fabricating highly hydrophobic surfaces that pin water droplets *Nano Lett.* **8** 1241–5

[60] Li Y, Zheng M, Ma L, M Zhong and Shen W 2008 Fabrication of hierarchical ZnO architectures and their superhydrophobic surfaces with strong adhesive force *Inorg. Chem.* **47** 3140–3